Limnol. Oceanogr., 59(4), 2014, 1297–1309
© 2014, by the Association for the Sciences of Limnology and Oceanography, Inc.
doi:10.4319/lo.2014.59.4.1297

Formation and erosion of biogeomorphological structures: A model study on the tube-building polychaete *Lanice conchilega*

Bas W. Borsje,[1,2,*] Tjeerd J. Bouma,[3] Marijn Rabaut,[4] Peter M. J. Herman,[3,5] and Suzanne J. M. H. Hulscher[1]

[1] Water Engineering and Management, University of Twente, Enschede, the Netherlands
[2] Deltares, Marine and Coastal Systems, Delft, the Netherlands
[3] Netherlands Institute of Sea Research (NIOZ-Yerseke), Yerseke, the Netherlands
[4] Marine Biology Section, Biology Department, Ghent University, Ghent, Belgium
[5] Faculty of Environmental Sciences, Radboud University Nijmegen, Nijmegen, the Netherlands

Abstract

We study how organism traits and population densities of ecosystem engineering species, in combination with environmental factors, affect the formation and erosion rates of biogeomorphological structures, and focus on the widely distributed marine tube-building polychaete *Lanice conchilega*, which lives in patches that form mounds up to 80 cm high in soft-bottom sediments. We modeled the tube-building worms as thin solid piles that affect drag and turbulence, and thereby the local sediment dynamics and thus mound dynamics. Hydrodynamic model predictions showed good agreement with flume experiments for flow-velocity adaptations both within and in front of a patch of tube-building worms. The modeled equilibrium mound height increased with the organism trait "tube length," and with population density, but was only little affected by the strength of the tidal current, water depth, and grain size. In all cases, the modeled mound heights were within the range of the mound heights observed in the field. The effect of the tube-building worm *L. conchilega* reached beyond the spatial scale of their biogenic structures, and persisted longer than the lifetime of the engineering organism itself.

There is a growing recognition of the importance of feedbacks between organisms and physical forces in landscape formation, which is generally referred to as biogeomorphology (Murray et al. 2008; Reinhardt et al. 2010; Corenblit et al. 2011). Biogeomorphological processes shape a broad range of landscapes, ranging from aeolian dunes (Baas and Nield 2007) and alluvial floodplain rivers (Murray and Paola 2003; Tal and Paola 2007) to tidal marshes (D'Alpaos et al. 2007; Kirwan and Murray 2007; Temmerman et al. 2007). Biogeomorphological processes typically involve so-called ecosystem engineering species, i.e., organisms that modify the abiotic environment via their physical structures or activity and thereby create, modify, and maintain habitats (Jones et al. 1994). Since the introduction of the concept a broad range of aspects that are affected by ecosystem engineering species has been studied (Jones et al. 1997, 2010). However, only recently the importance of the persistence of structures created by ecosystem engineering species has been recognized (Hastings et al. 2007; Jones et al. 2010; Jones 2012). In addition to that, little attention has been given in the field of biogeomorphology on how organism traits (Bouma et al. 2005, 2010; Peralta et al. 2008) and population density (Bouma et al. 2007; Van Hulzen et al. 2007; Widdows and Brinsley 2002) of ecosystem engineering species affect biogeomorphological landscape formation. As a result, there is currently a general lack of knowledge on how organism traits of ecosystem engineering species in combination with population density and environmental factors affect the formation and erosion rates of biogeomorphological structures and landscapes.

Coastal ecosystems are ideal to study how the dynamics of biogeomorphological structures are affected by organism traits of ecosystem engineering species. Not only do a broad range of ecosystem engineering species interact with hydrodynamics and sediment dynamics within these systems (Widdows and Brinsley 2002), but also the range of environmental factors that these organisms may encounter is wide (Herman et al. 2001; Degraer et al. 2003). Moreover, the recent progress made in modeling biogeomorphological interactions using process-based models (Le Hir et al. 2007; Borsje et al. 2008; Orvain et al. 2012) allows in-depth study of these systems. The main biogeomorphological interactions in these ecosystems involve stabilization or destabilization of the sediment by biological activity, which can modify sediment transport rates by a factor of 2 and more, compared with the purely physical case (Graf and Rosenberg 1997; Widdows and Brinsley 2002).

In our study we focus on the widely distributed tube-building worm, *Lanice conchilega*, as a model species. *L. conchilega* is an ecosystem engineering species that lives in patches and creates rigid tubes that protrude several centimeters from the sediment into the water column, whereas most of the tube remains hidden in the seabed (Van Hoey 2006). The protruding tubes directly influence the near-bed water flow and thereby the sediment dynamics (Eckman et al. 1981). Coverage density of these tube-building worms is defined as the ratio of surface area occupied by the tubes to the total patch area. Coverage densities up to 40% have been recorded in the field (Nicolaidou 2003). Flume experiments (Friedrichs et al.

* Corresponding author: b.w.borsje@utwente.nl

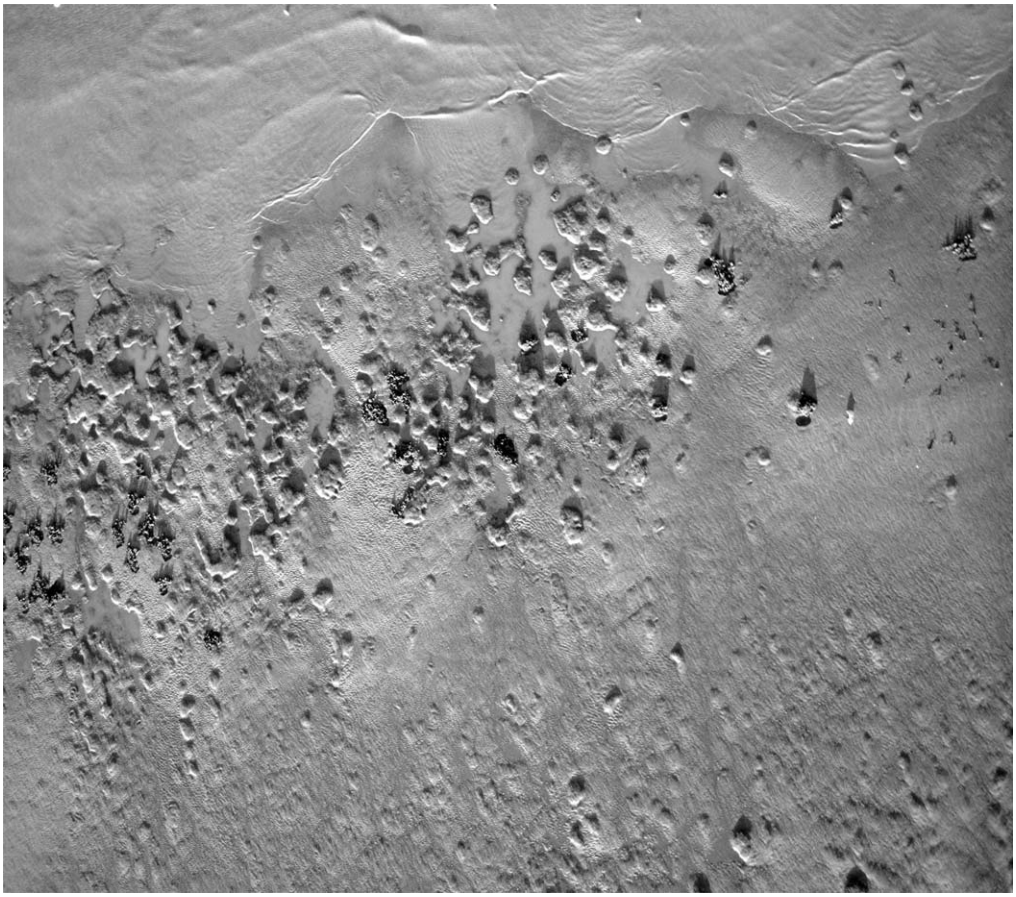

Fig. 1. Aerial picture of intertidal area with *Lanice conchilega* reefs. Total area is approximately 100 × 100 m. Picture taken with camera Canon D10 attached to a kite. Intertidal area of Boulogne-sur-Mer during spring low tide; 14 October 2011. Picture courtesy of Klaas Pauly and Marijn Rabaut, Ghent University.

2000, 2009; Friedrichs and Graf 2009) have shown that coverage densities $> 5\%$ cause sediment stabilization by skimming flow, whereas at lower coverage densities erosion may be enhanced through turbulence. Field studies have shown that patches of *L. conchilega* indeed raise the seabed by sediment trapping in between the protruding tubes (Fig. 1). By extending the tubes after sedimentation, *L. conchilega* mounds can reach a height of 7.5 to 80 cm above the surrounding seabed (Carey 1987; Degraer et al. 2008; Rabaut et al. 2009). The growth rates of the tubes themselves are up to 1.5 mm h^{-1} (Rabaut 2009). In contrast to the flume experiments, field observations showed sediment stabilization and hence mound formation for coverage densities as low as 1% (Rabaut et al. 2009).

Recently, the effect of tube-building worms has been included in large-scale geomorphological models, showing that the local stabilizing effect of dense patches of tube-building worms can affect the large-scale sediment transport (Bobertz et al. 2009; Borsje et al. 2009*a*,*b*). However, because these studies only used simplified empirical relations between the population density of tube-building worms and their effect on bed roughness, they cannot reproduce the trapping of sediment by the protruding tubes and consequently mound formation by *L. conchilega*.

In this study, we aim to provide a mechanistic understanding of the formation and erosion rates of the *L. conchilega* mounds. Specifically, we focus on how the formation and erosion rates of these mounds depend on protruding tube length (an organism trait), population density, and environmental factors. Therefore, we used a numerical shallow water model (Delft3D) extended with a module that accounts for the influence of rigid cylindrical structures on drag and turbulence (Dijkstra and Uittenbogaard 2010). This model enabled us to explicitly account for the interactions among the tubes, the hydrodynamics, and the sediment dynamics.

Methods

Model description—The formation and erosion of mounds were modeled using the numerical shallow water model Delft3D (Lesser et al. 2004). The system of equations consists of the horizontal momentum equations, a continuity equation, a turbulence closure model, a sediment transport equation, and a sediment continuity equation (Borsje et al. 2013). The vertical momentum equation is reduced to the hydrostatic pressure relation as vertical accelerations are assumed to be small compared with

gravitational acceleration. The model equations are solved by applying vertical sigma layering (Deltares 2014).

In terms of the sigma coordinates, the hydrostatic shallow water equations are described by:

$$\frac{\partial u}{\partial t}+u\frac{\partial u}{\partial x}+v\frac{\partial u}{\partial y}+\frac{\omega}{H}\frac{\partial u}{\partial \sigma} =-\frac{1}{\rho_w}P_u+F_u+\frac{1}{(H)^2}\frac{\partial}{\partial \sigma}\left(\upsilon\frac{\partial u}{\partial \sigma}\right) \quad (1)$$

$$\frac{\partial v}{\partial t}+u\frac{\partial v}{\partial x}+v\frac{\partial v}{\partial y}+\frac{\omega}{H}\frac{\partial v}{\partial \sigma} =-\frac{1}{\rho_w}P_v+F_v+\frac{1}{(H)^2}\frac{\partial}{\partial \sigma}\left(\upsilon\frac{\partial v}{\partial \sigma}\right) \quad (2)$$

$$\frac{\partial \omega}{\partial \sigma}=-\frac{\partial \zeta}{\partial t}-\frac{\partial Hu}{\partial x}-\frac{\partial Hv}{\partial y} \quad (3)$$

Here, u is the horizontal velocity in x direction, v is the horizontal velocity in y direction, ω is vertical velocity relative to the moving vertical sigma plane, ρ_w is the water density, H is total water depth, P is the pressure gradient, F is the horizontal Reynolds stress, and υ is the vertical eddy viscosity. The vertical eddy viscosity υ is calculated by means of the k-ε turbulence closure model in which both the turbulent energy k and the dissipation ε are computed. The Delft3D model contains a module that explicitly accounts for the influence of cylindrical structures on drag and turbulence by an extra source term of friction force in the momentum equation and an extra source term of total kinetic energy and turbulent energy dissipation in the turbulence closure model. Details on the equations and the calibration tests of this module are given by Temmerman et al. (2005) and Dijkstra and Uittenbogaard (2010).

After the flow field is calculated, the total sediment transport rates are computed. In the model, the sediment transport is split into two components: bedload transport and suspended load transport. The bedload transport in x direction $S_{b,x}$ is calculated by (Van Rijn et al. 2004):

$$S_{b,x}=0.006\rho_s w_s d\ M^{0.5}M_e^{0.7} \quad (4)$$

where ρ_s is the density of the sediment, w_s is the settling velocity of the sediment, and d the sediment grain size. The sediment mobility number M and the excess sediment mobility number M_e are given by:

$$M=\frac{u_r^2}{(\rho_s/\rho_w-1)gd} \quad (5)$$

$$M_e=\frac{\left(u_r-S_{cr}\right)^2}{(\rho_s/\rho_w-1)gd} \quad (6)$$

where u_r is computed from the velocity profile in the bottom computational layers and S_{cr} is the critical velocity for the initiation of motion of sediment based on the Shields curve. If $u_r < S_{cr}$ the bedload transport in x direction is set to zero. The bedload transport in y direction $S_{b,y}$ is calculated with the same equations (Eqs. 4–6), only based on v_r computed from the velocity profile in y direction.

The suspended sediment concentration is calculated by solving the advection–diffusion equation:

$$\frac{\partial c}{\partial t}+\frac{\partial cu}{\partial x}+\frac{\partial cv}{\partial y}+\frac{\partial (w-w_s)c}{\partial z} =\frac{\partial}{\partial x}\left(\varepsilon_{s,x}\frac{\partial c}{\partial x}\right)+\frac{\partial}{\partial y}\left(\varepsilon_{s,y}\frac{\partial c}{\partial y}\right)+\frac{\partial}{\partial z}\left(\varepsilon_{s,z}\frac{\partial c}{\partial z}\right) \quad (7)$$

where c is the mass concentration of sediment and $\varepsilon_{s,x}$, $\varepsilon_{s,y}$, and $\varepsilon_{s,z}$ are the sediment diffusivity coefficients in x, y, and z direction, respectively.

Suspended sediment includes all sediment transported above the reference height, $a = 0.01H$. The reference concentration, c_a at height a, is given by (Van Rijn 2007):

$$c_a=0.015\rho_s\frac{dT_a{}^{1.5}}{aD_*{}^{0.3}} \quad (8)$$

Here, T_a is the non-dimensional bed shear stress:

$$T_a=\frac{u_c\tau_b-\tau_{cr}}{\tau_{cr}} \quad (9)$$

where u_c is the efficiency factor, which is the ratio between the grain-related friction factor and the total current-related friction factor, τ_{cr} the critical bed shear stress for the initiation of motion of sediment, and D_* is the non-dimensional particle diameter. The bed shear stress τ_b is calculated by:

$$\tau_b=\rho_w u_*^2 \quad (10)$$

where u_* is the bed shear velocity. For details on the calculation of suspended sediment concentrations *see* Borsje et al. (2014).

Finally, the bed evolution is governed by the sediment continuity equation, which reads:

$$\left(1-\varepsilon_p\right)\frac{\partial z_b}{\partial t}+\frac{\partial\left(S_{b,x}+S_{s,x}\right)}{\partial x}+\frac{\partial\left(S_{b,y}+S_{s,y}\right)}{\partial y}=0 \quad (11)$$

in which $\varepsilon_p = 0.4$ is the bed porosity, S_b is the bedload transport (Eq. 4), and S_s is the suspended load transport, calculated by:

$$S_{s,x}=\int_a^H\left(uc-\varepsilon_{s,z}\frac{\partial c}{\partial x}\right)dz \quad (12)$$

$$S_{s,y}=\int_a^H\left(vc-\varepsilon_{s,z}\frac{\partial c}{\partial y}\right)dz \quad (13)$$

Equation 11 simply states that convergence (or divergence) of the total transport rate must be accompanied by a rise (or fall) of the bed profile.

Flume experiments for model validation—To understand the effect of tube patches on hydrodynamics and gradients

in sediment transport, it is necessary to characterize flow velocities within as well as upstream and downstream of tube patches. Data on flow velocity variations within a patch of tube-building worms with varying population density were obtained from a flume experiment by Friedrichs et al. (2000). Data on flow velocity variations at various distances upstream of a patch of tube-building worms were obtained from an additional flume experiment. Experimental data from both flume experiments were then used for model validation.

The flume experiment by Friedrichs et al. (2000) was executed in a recirculating flume with a width of 0.40 m, a height of 0.40 m, and a working channel of 3 m length. During the experiment, the water depth was kept constant at 0.20 m and the free-stream flow velocity was set to 0.05 m s^{-1}. The artificial tubes were 5 cm in length, 0.5 cm in diameter, and protruded 3.5 cm into the water column, i.e., mimicking *L. conchilega* tubes. The tubes were distributed regularly over a length of 28 cm and the full width of the flume. The flow deceleration within the tube field was measured for four different tube densities: 3836, 1961, 872, and 490 individuals per square meter (ind. m^{-2}) at the end of the 28 cm long patch. Corresponding coverage densities were: 8.8%, 4.5%, 2.0%, and 1.1%, and thereby comparable with coverage densities found in the field. The flume experiment was run without tubes to obtain a reference flow velocity at $z = 1.5$ cm above the bed. The flow velocity for the different tube densities was measured at $z = 1.5$ cm above the bed at different positions within the patch. The flow deceleration was then expressed in percentage of the reference velocity.

Flow velocity variations upstream of a patch of *L. conchilega* mimics with varying tube densities (3264, 2448, and 1632 ind. m^{-2}) were measured in a large racetrack flume at the Netherlands Institute of Sea Research (NIOZ-Yerseke). Corresponding coverage densities were: 6.4%, 4.8%, and 3.2%. This large racetrack flume (total volume of about 9 m^3) consists of an oval channel (0.6 m wide $\times$ 0.5 m high) with a total length of 17.5 m, and a straight working section of 10.8 m, providing ample length to measure hydrodynamics upstream of the patch. The bed was composed of fine sand with a median grain size of 0.2 mm, and we used salt water with a density of 1020 kg m^{-3} and a water temperature of 15°C. For further details on the racetrack flume *see* Bouma et al. (2005). During the experiment, the water depth was maintained at 0.20 m and a free-stream velocity of 0.25 m s^{-1} was generated by a conveyor belt system, acting as a paddle wheel. Flow measurements were carried out with a Nortek acoustic doppler velocimeter (ADV) set to operate at a rate of 10 Hz. The ADV was mounted on a computerized three-dimensional (3D) positioning system, which was mounted on a carriage that could be placed anywhere along the length of the working section. Horizontal velocities were measured at three positions (30 cm, 15 cm, and 0 cm before the leading edge) and at three different heights ($z = 2$ cm, $z = 5$ cm, and $z = 10$ cm) above the bed.

In the test section of the flume (2 m long, 0.6 m wide) we placed 7 cm long rigid drinking straws (0.5 cm diameter) from which 3.5 cm length protruded into the water column (Friedrichs et al. 2000). The patch size of the straws was 0.6 m in width and 0.49 m in length. To construct an even but non-regular distribution of the tubes, a grid was placed with a mesh size of 3.5 $\times$ 3.5 cm on the bed of the flume. Within every mesh of the grid four tubes with a different color were placed randomly. This resulted in an even distribution at a scale $>$ 3.5 cm, but with random interindividual distances at the smaller scale. By removing one color from the patch the population density of the patch was reduced, but still evenly and non-regularly distributed over the area. The spatial layout of a non-regular distribution was to mimic field observations realistically, whereas previous flume experiments used a regular distribution with fixed distances between straws (Friedrichs et al. 2000, 2009; Friedrichs and Graf 2009). Although the water depth was identical in both flume experiments ($H = 0.20$ m), the free-stream flow velocity was different in both flume experiments. In the new flume experiment, we aimed to mimic field observations more realistically and therefore imposed a larger free-stream velocity. The imposed free-stream velocity of $u = 0.25$ m s^{-1} produced a bed shear stress, which was just below the critical bed shear stress for erosion.

Model setup—In the model setup, the x direction was in the direction of the flow. The y direction was perpendicular to the x direction and the z direction was pointing upward from the bed. Two different model setups were used: (1) to validate the model with the flume experiments and (2) to simulate field conditions. The former was set up in a two-dimensional (2D) mode, i.e., considering flow and variation in two dimensions only (x and z direction) and the latter in three dimensions, i.e., considering flow and variation in x, y, and z directions.

The horizontal model domain of the 2D model was 60 m, with a constant resolution of 0.15 m (400 horizontal grid cells). In the vertical, the model grid was composed of 100 layers, with small vertical grid steps near the bed and increasing toward the water surface. At the upstream boundary a flow velocity was imposed, whereas at the downstream boundary a water depth was imposed of $H =$ 0.2 m. The model boundaries were chosen far away from the area of interest to avoid boundary effects, and the model domain was therefore not the same as the total length of the flume. To compare the model results with the new flume experiments, the unidirectional free-stream flow velocity was set to $U_{uni} = 0.25$ m s^{-1}, whereas the unidirectional free-stream flow velocity was set to $U_{uni} =$ 0.05 m s^{-1} to compare the model results with the flume experiment executed by Friedrichs et al. (2000). The bottom roughness height was set to $k_s = 7 \times 10^{-4}$ m, on the basis of flow measurements in the flume without tubes (Bouma et al. 2007). In the center of the model domain vertical rigid cylinders were defined over a section of 2.5 m, each with a tube diameter $d_{tube} = 0.5$ cm, a tube length varying between $L_{tube} = 2.0$ cm and 3.5 cm, and a tube density varying between $D_{tube} = 0$ ind. m^{-2} and 5000 ind. m^{-2}. The tube length L_{tube} was defined as the length of the tube protruding into the water column.

Table 1. Parameter settings for the hydrodynamic model simulations.

	Symbol (unit)	Inside patch Fig. 2	Outside patch Fig. 3	Field conditions Fig. 4
Flow velocity	U_{uni} (m s^{-1})	0.05	0.25	0.25
Water depth	H (m)	0.2	0.2	2
Roughness height	k_s (m)	7×10^{-4}	7×10^{-4}	6×10^{-3}
Tube diameter	d_{tube} (cm)	0.5	0.5	0.5
Tube length	L_{tube} (cm)	2.0, 3.5	3.5	3.5
Tube density	D_{tube} (ind. m^{-2})	0–5000	0–5000	500, 5000

The horizontal model domain of the 3D model was 50 m $\times$ 50 m, with a variable resolution of 0.33 $\times$ 0.33 m in the center of the domain increasing to 1 $\times$ 1 m toward the lateral boundaries (4900 horizontal grid cells). In the vertical, the model grid was composed of 20 layers, with small vertical steps near the bed and increasing toward the water surface. The default water depth was set to H = 2 m, and a bidirectional tidal flow was imposed, which changed in direction every 6 h and had a maximum velocity of U_{M2} = 0.5 m s^{-1}. The tidal flow produced a bed shear stress, which was above the critical bed shear stress for erosion during most of the tidal period. The bottom roughness height was set to $k_s = 6 \times 10^{-3}$ m. All settings represented typical field conditions (Verfaille et al. 2006; Bouma et al. 2007; Degrear et al. 2008). The bottom roughness height mimicking field conditions was much larger compared with the bottom roughness height mimicking the flume experiments, since the bed in the flume was nearly flat and the bed in the field usually shows small-scale geomorphological features like sand ripples (Fig. 1). In the center of the model domain vertical rigid cylinders were defined over a section of 2 $\times$ 2 m, each with a diameter of d_{tube} = 0.5 cm, a tube length varying between L_{tube} = 1.0 cm and 4.0 cm, and a tube density varying between D_{tube} = 0 ind. m^{-2} and 5000 ind. m^{-2}.

We ran the model until an equilibrium mound height (h_{eq}) was reached. The equilibrium mound height was reached when the morphological changes within an hour were smaller than 1%. The time to reach the equilibrium mound height is defined as the equilibrium time (T_{eq}). In all model simulations, the tubes themselves had the same growth rate as the formation rate of the mounds and therefore always protruded into the water column with the same length. In the model simulations, a geomorphological acceleration factor (MORFAC) of 60 was used to speed up the geomorphological changes (Deltares 2014). By using a MORFAC of 60 the deposition and erosion fluxes were multiplied by a factor 60 after each time step. After each time step the bed level was updated and the new flow field was calculated. Consequently, one time step corresponds to 3 s $\times$ 60 = 3 min of geomorphological changes. A smaller MORFAC value showed the same equilibrium mound height and equilibrium time for a test simulation but required longer simulation times.

Overview of model simulations—To understand the formation and erosion of mounds, we use the following outline. (1) We present the model results on hydrodynamics and start with the validation of the model both within and in front of a patch of tube-building worms for a flat bed. Moreover, we model the effect of the tube-building worms on the 3D flow field. All the parameter settings for the hydrodynamic model simulations are listed in Table 1. (2) We show the geomorphological development in time of a patch of tube-building worms for the parameter settings listed in Table 2. This simulation is labeled as the reference run. (3) We investigate the sensitivity in mound height and equilibrium time for a variation in tube length, tube density, flow velocity amplitude, water depth, grain size, and absence of tubes, according to the parameter settings listed in Table 2 and all relative to the reference run.

Results

Hydrodynamic effects of L. conchilega *patches—measurements and modeling*—Within a patch of tube-building worms we found that flow velocity decreased fast with increasing tube density as long as tube densities are lower

Table 2. Parameter settings for the geomorphodynamic model simulations. Bold numbers indicate dynamic variables in model simulations.

		Reference run	Tube length	Tube density	Physical factors			Mound erosion
	Symbol (unit)	Fig. 5	Fig. 6	Fig. 7	Fig. 8A,B	Fig. 8C,D	Fig. 8E,F	Fig. 9
Tidal flow amplitude	U_{M2} (m s^{-1})	0.50	0.50	0.50	**0.40–0.60**	0.50	0.50	0.50
Water depth	H (m)	2	2	2	2	**1–3**	2	2
Grain size	d (mm)	0.2	0.2	0.2	0.2	0.2	**0.1–0.3**	0.2
Roughness height	k_s (m)	6×10^{-3}	6×10^{-3}	6×10^{-3}	6×10^{-3}	6×10^{-3}	6×10^{-3}	6×10^{-3}
Tube diameter	d_{tube} (cm)	0.5	0.5	0.5	0.5	0.5	0.5	
Tube length	L_{tube} (cm)	2.0	**1.0–4.0**	2.0, 4.0	2.0	2.0	2.0	
Tube density	D_{tube} (ind. m^{-2})	500	500	**0–5000**	500	500	500	

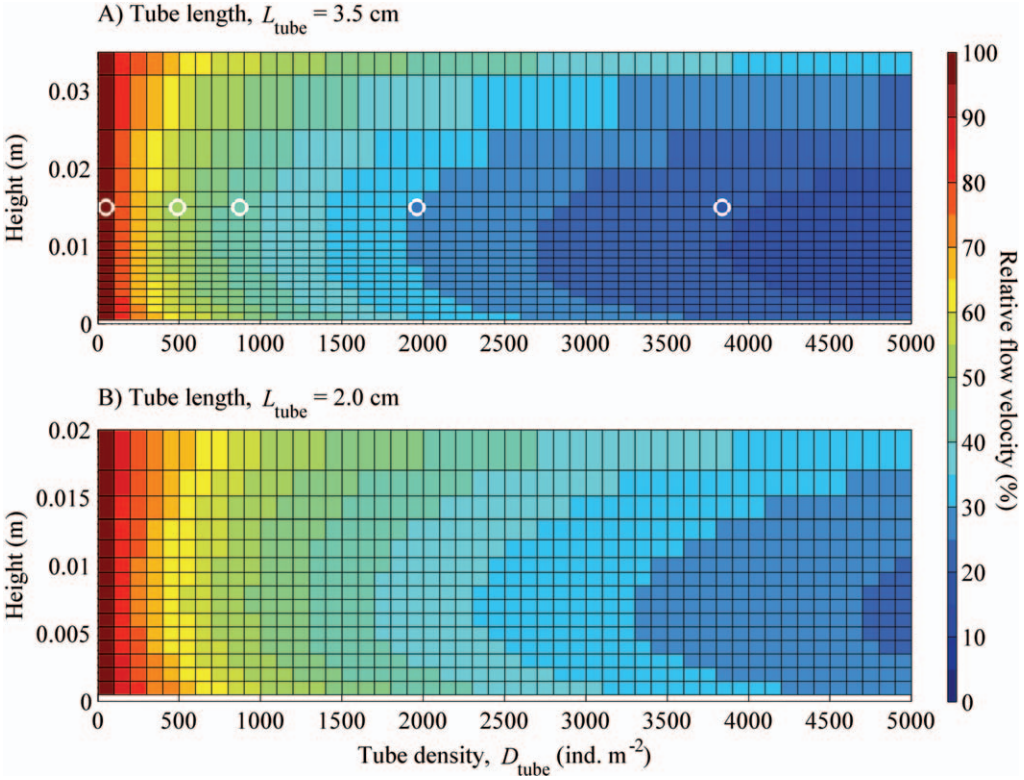

Fig. 2. Relative flow velocity (%) at 28 cm downstream of the leading edge for a tube length (A) L_{tube} = 3.5 cm and (B) L_{tube} = 2.0 cm and flat bed. Results are given at different heights (m) above the sediment bed and for increasing tube densities D_{tube} (ind. m^{-2}). Circles are flume measurements (Friedrichs et al. 2000) and areas are derived from model simulations. In both cases, flow velocity is expressed as percentage of a reference velocity at 1.5 cm height over bare sediment, using a color scale from 0% (i.e., flow = 0 m s^{-1}) to 100% (i.e., no flow deceleration) for visualization.

than D_{tube} = 1000 ind. m^{-2} (Fig. 2). For tube densities of D_{tube} = 5000 ind. m^{-2} and a tube length of L_{tube} = 3.5 cm, the modeled flow deceleration reached a constant value of around 15% of the reference velocity at 1.2 cm height (Fig. 2A). However, for a tube length of L_{tube} = 2.0 cm and a tube density of D_{tube} = 5000 ind. m^{-2}, the flow deceleration reached a value of around 25% at 0.6 cm height and was still decreasing with tube density (Fig. 2B). The model results showed that the flow deceleration was not uniform over the height; the maximum flow deceleration was between 1.0 cm and 1.5 cm height for 3.5 cm tubes and between 0.5 and 0.7 cm height for 2.0 cm tubes. Comparison of our model results (Fig. 2A: area) with results from the flume experiment by Friedrichs et al. (2000; Fig. 2A: circles) showed good agreement for the flow deceleration within a patch of tube-building worms.

Modeling a range of tube densities showed that the current velocities were affected far beyond the tube patch itself. Both at 30 cm and 15 cm upstream of the patch, the flow velocities gradually increased near the bed (up to around 7 cm above the bed) for increasing tube density (Fig. 3). However, at the leading edge (i.e., 0 cm in front of the patch) the flow velocity was strongly reduced near the bed and slightly underpredicted by the model for high densities. Higher in the water column (higher than around 7 cm above the bed), the opposite trend was observed: flow velocities decreased for increasing tube densities at 30 cm and 15 cm in front of the patch, whereas at the leading edge the flow velocities increased for increasing tube densities. The trend can be explained by the continuity of the water flow: decreasing flow velocities near the bed are compensated by increasing flow velocities higher in the water column and vice versa. Again, there was good agreement between the modeled (Fig. 3: area) and measured (Fig. 3: circles) hydrodynamic effects of the tube-building worms in front of the patch.

Subsequently, we modeled the effect of the tube-building worm patch in 3D for two different tube densities (D_{tube} = 500 ind. m^{-2} and 5000 ind. m^{-2}) and a tube length L_{tube} = 3.5 cm under field conditions (Fig. 4). In both simulations the maximum value of vertical velocity w in front of the patch was around 10 times larger than the maximum horizontal cross-patch velocity v around the patch. The interaction between the patch and the environment clearly showed both a stabilizing and a destabilizing effect (i.e., a decrease and increase in bed shear stress respectively; Fig. 4E,F). The stabilization and destabilization was stronger for the high tube density simulation. For both tube densities, the flow within the patch was reduced as shown before (Fig. 2). However, the flow over the patch (height $>$ 0.25 m) was accelerated due to continuity, resulting in an uplift of water close to the front of the patch (Fig. 4C,D). This, in turn, caused an acceleration of horizontal flow just in front of the uplifting water. The

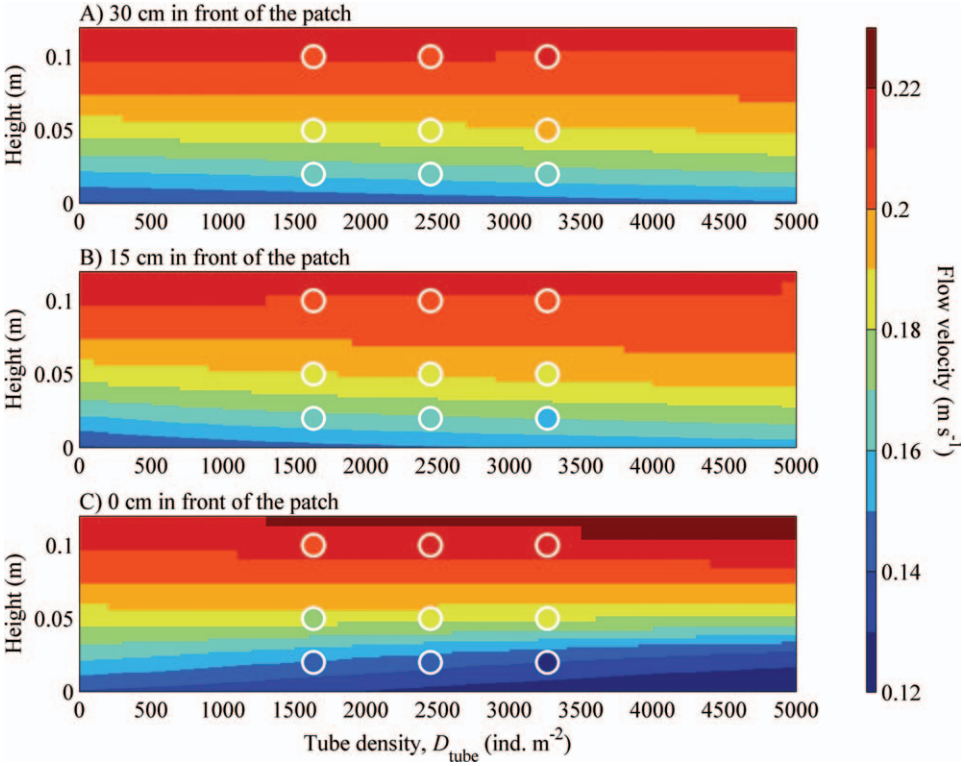

Fig. 3. Flow velocity (m s^{-1}) at (A) 30 cm, (B) 15 cm, and (C) 0 cm in front of a patch with a tube length L_{tube} = 3.5 cm and a flat bed. Results are given at different heights (m) from the bed and for increasing tube densities D_{tube} (ind. m^{-2}). Circles are flume measurements and areas are derived from model simulations.

result was an increase in bed shear stress in front of the patch and a reduction of the bed shear stress within the patch (Fig. 4E,F). In the wake zone of the patch the bed shear stress was also reduced over a long distance. Remarkably, the footprint of a tube-building worm patch (defined as the area for which the bed shear stress is influenced by more than 10% compared with the bed shear stress without tubes) was 2.9 for a tube density of D_{tube} = 500 ind. m^{-2} and 5.3 for a tube density of D_{tube} = 5000 ind. m^{-2}. The flow was mostly deflected over the patch (Fig. 4C,D), and partly around the patch (Fig. 4A,B).

Modeling geomorphodynamics of L. conchilega *patches—variation in tube length and tube density*—Modeling the mound formation by tube-building worms showed that the geomorphological changes are the largest in the first weeks, during which large amounts of sediment were deposited within and around the patch (Fig. 5). Since the location of the leading edge switches during the tidal period, the erosion at the leading edge during the first half of the tidal period was compensated by the accretion of sediment during the second half of the tidal period. Because of the increase in bed level within the patch, the flow velocity also increased over and within the patch due to continuity of the water flow. Over time, the sediment transport rate on top of the mound equaled the sediment transport rate around the patch, so that an equilibrium mound height h_{eq} was reached after 160 d for this parameter setting. Remarkably, the mound extended largely around the patch. The mound extended over 14 m and 6 m in the flow direction and in the cross-flow direction, respectively. The shape of the mounds derived from numerical simulations have to be interpreted with some caution because a simplified bidirectional current regime was applied in the model, whereas in nature current directionality may change in all directions over the tidal cycle.

Subsequently, we modeled the mound formation by tube-building worm patches of four contrasting tube lengths (L_{tube} = 1.0 cm to 4.0 cm). The equilibrium mound height h_{eq} showed an almost linear relation with tube length L_{tube} (Fig. 6): $h_{eq} = 10.3 \times L_{tube}$ (R^2 = 0.96). This was remarkable, as for a tube density of D_{tube} = 500 ind. m^{-2} there was only 10% difference in flow deceleration between the longer tubes (i.e., 65% deceleration; Fig. 2A) and the shorter tubes (i.e., 55% deceleration; Fig. 2B). This indicated that the relation between flow deceleration and geomorphodynamic changes was nonlinear.

Next, we used the model to quantify how the equilibrium mound height h_{eq} and equilibrium time T_{eq} depended on tube density (D_{tube} from 0 ind. m^{-2} to 5000 ind. m^{-2}) for two contrasting tube lengths (L_{tube} = 2.0 cm and 4.0 cm). As the gradient in flow deceleration was most sensitive to tube density changes at low tube densities (Fig. 2), the equilibrium mound height h_{eq} and equilibrium time T_{eq} also showed the highest sensitivity to variations in tube densities at low tube densities (Fig. 7). For high tube densities (D_{tube} > 3000 ind. m^{-2}), the equilibrium mound height h_{eq} hardly increased with further increasing tube densities, resulting in

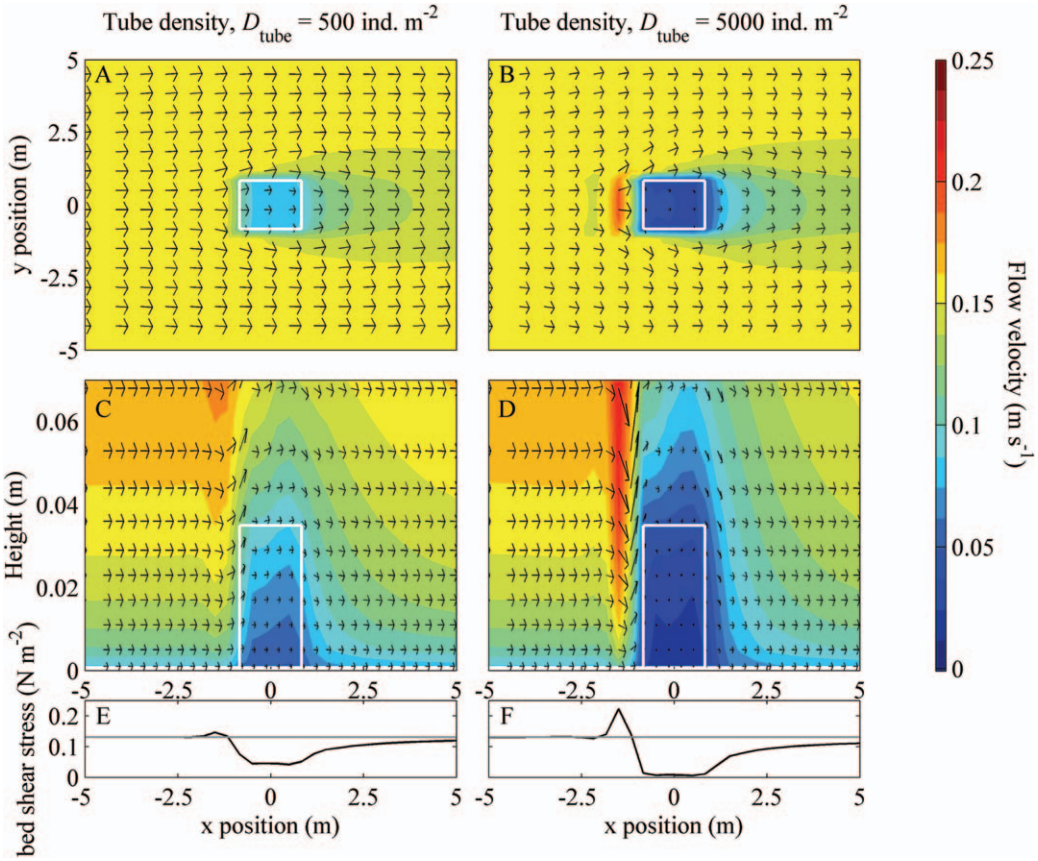

Fig. 4. Interaction between a patch of 3.5 cm long tube-building worms (framed box) and the environment, for a patch size of 2 × 2 m and a tube density (A, C, E) D_{tube} = 500 ind. m^{-2} and (B, D, F) D_{tube} = 5000 ind. m^{-2} and a flat bed. (A, B) Top view of the horizontal flow velocity u (m s^{-1}) at a height of z = 3.0 cm from the bed, (C, D) side view of the horizontal flow velocity u (m s^{-1}) in the center of the patch (y = 0 m), and (E, F) bed shear stress (N m^{-2}) in the center of the patch (y = 0 m). Arrows indicate (A, B) flow velocity vectors' (u, v) strength and angle and (C, D) flow velocity vectors' (u,w) strength and angle. For visualization purpose the cross-patch velocity component v and vertical flow velocity component w are multiplied by a factor of 5.

a maximum mound height for a given flow velocity amplitude U_{M2}, water depth H, and grain size d. In this case, the maximum equilibrium mound height h_{eq} = 0.35 m and h_{eq} = 0.70 m for a tube length of L_{tube} = 2.0 cm and L_{tube} = 4.0 cm, respectively.

Modeling geomorphodynamics of L. conchilega *patches—physical factors*—The model allowed us to quantify the sensitivity in equilibrium mound height h_{eq} and equilibrium time T_{eq} for a range of flow velocity amplitudes U_{M2}, water depths H, and grain sizes d (Fig. 8), relative to the reference run (gray circle; Fig. 6). By increasing the flow velocity amplitude U_{M2}, the equilibrium mound height h_{eq} hardly changed (Fig. 8A), since the flow deceleration within the patch was almost the same for the different flow velocity amplitudes. However, the equilibrium time T_{eq} decreased for increasing flow velocity amplitude (Fig. 8B) due to the increase in total transport rate. For increasing water depth H, the equilibrium mound height h_{eq} increased (Fig. 8C), because the flow acceleration on top of the patch became smaller, causing lower sediment transport rates within the patch. Consequently, also the equilibrium time T_{eq} increased with increasing water depth (Fig. 8D). For a variation in grain size d we observed two trends. First, starting from a small grain size, the equilibrium mound height h_{eq} increased and the equilibrium time decreased for increasing grain size (i.e., from d = 0.1 to 0.2 mm). However, for larger grains (d > 0.2 mm) the opposite trend was observed (Fig. 8E). For small grain sizes, suspended load transport is the dominant transport mode. In this regime, the small grain sizes were easily picked up from the bed, even within the patch. Consequently, the equilibrium mound height h_{eq} was smaller compared with the reference run. The equilibrium time T_{eq} was long in the suspended load transport regime, since the sediment was mostly transported over and along the patch. In contrast, for large grain sizes bedload is the dominant transport regime, and the equilibrium mound height h_{eq} was comparable with the reference run (Fig. 6: L_{tube} = 2.0 cm). Nevertheless, the equilibrium time T_{eq} is much longer for the larger grain size, since the total transport rate was much smaller (Fig. 8F). For the other simulations (Fig. 8A–D), the transport regimes were all within the incipient suspended load transport regime.

Modeling geomorphodynamics of Lanice conchilega *patches—erosion*—Finally, the model allowed us to study the erosion of the mounds, once the tube-building worms

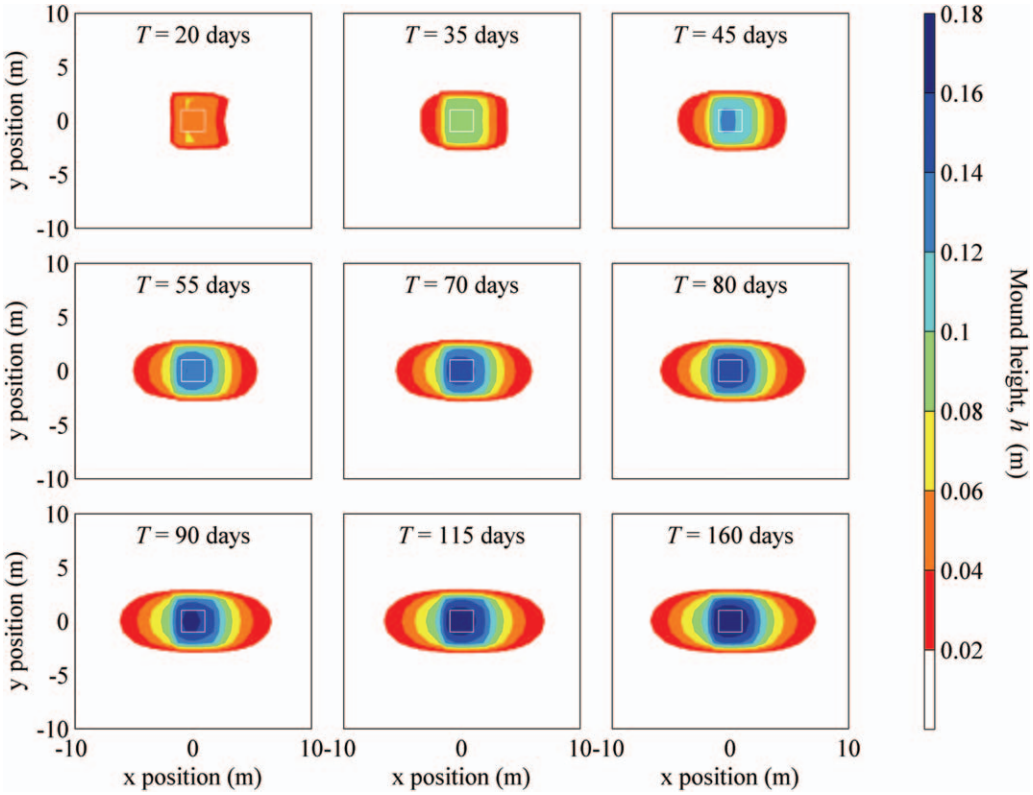

Fig. 5. Top view of the geomorphological development for a 2 × 2 m patch (framed box) with a tube density D_{tube} = 500 ind. m^{-2} and a tube length L_{tube} = 2.0 cm (reference run). Mound heights (m) are given during flood (i.e., maximum flow in positive x direction).

had disappeared because of, e.g., recruitment failure. As initial topography we used the equilibrium mound height reached for a tube density D_{tube} = 500 ind. m^{-2} and a tube length L_{tube} = 2.0 cm and L_{tube} = 4.0 cm (Fig. 6). In the first weeks the mound height decreased rapidly (Fig. 9), but later the rate slowed and the time needed to flatten the mound (Fig. 9) was comparable with the time needed to form the mound (Fig. 6).

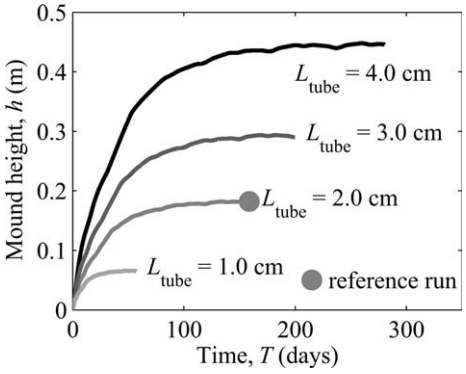

Fig. 6. Mound formation for a tube density D_{tube} = 500 ind. m^{-2} and tube lengths varying between L_{tube} = 1.0 cm and 4.0 cm. The small irregularities in mound height (h) during growth are caused by the used MORFAC.

Discussion

We addressed the question of how organism traits and population density of ecosystem engineering species interact with environmental factors to affect the rates of formation and erosion of biogeomorphological structures. The use of a physically sound model of hydrodynamics and sediment transport offered us a unique tool to quantify these processes for biogeomorphological mound formation by the tube-building worm *L. conchilega*. After validating the model against flume measurements, we demonstrated that the formation and erosion rates mainly depended on tube length and population density, whereas environmental factors (flow velocity amplitude, water depth, and grain size) were less important. As already shown for other ecosystem engineering species (Hastings et al. 2007), we showed that the effect of the tube-building worm *L. conchilega* reached beyond the spatial scale of their biogenic structures (Fig. 5), and persisted longer than the lifetime of the engineering organism itself (Fig. 9).

The modeled mound heights were in the range of 6–70 cm and were formed within 55–450 d. The geomorphological development was the largest in the first couple of days, in which growth rates of the mounds were in the order of 1 mm h^{-1} (Fig. 6). The growth rates of the tubes themselves are up to 1.5 mm h^{-1} (Rabaut 2009), and the tubes are therefore able to follow the growth of the mound. The mound heights measured in the field were in the range of 7.5 to 80 cm (Carey 1987; Degraer et al. 2008; Rabaut

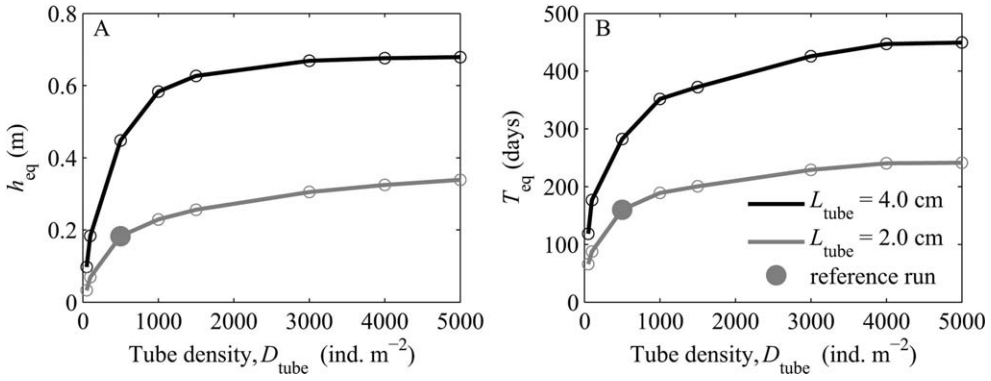

Fig. 7. (A) Equilibrium mound height (h_{eq}) and (B) equilibrium time (T_{eq}) for increasing tube densities D_{tube} and for a tube length L_{tube} = 2.0 cm and 4.0 cm.

et al. 2009) and thereby similar to the mound heights modeled. The mound heights measured by Degraer et al. (2008) and Rabaut et al. (2009) in the Belgium coastal zone were in the range of 7.5–16.5 cm and were measured in winter and in the period between May and June. *L. conchilega* populations show a recruitment period from spring to late autumn, after which the adult population starts to die off, leading to erosion of the mounds (Carey 1987; Degraer et al. 2008). Therefore, the modest mound heights measured in the Belgium coastal zone might be explained by measuring the mounds in a period of erosion of the mound (Degraer et al. 2008) or at the start of the recruitment period, when the tube lengths are still small (Rabaut et al. 2009). Carey (1987) studied the seasonal variation in mound heights for 3 yr at a beach at the English coastal zone. The largest mound heights were measured between September and the start of October, when mound heights up to 80 cm were measured.

Our model predictions are limited to simulations of flow-dominated subtidal environments. This constitutes a natural habitat for the tube-building worm *L. conchilega* (Rabaut et al. 2007), but the species also occurs intertidally. Our model cannot simulate this accurately, as the drying and flooding may generate numerical problems in the results if the gradient in bed level is quite large, as is the case for mounds. Field studies showed that mound

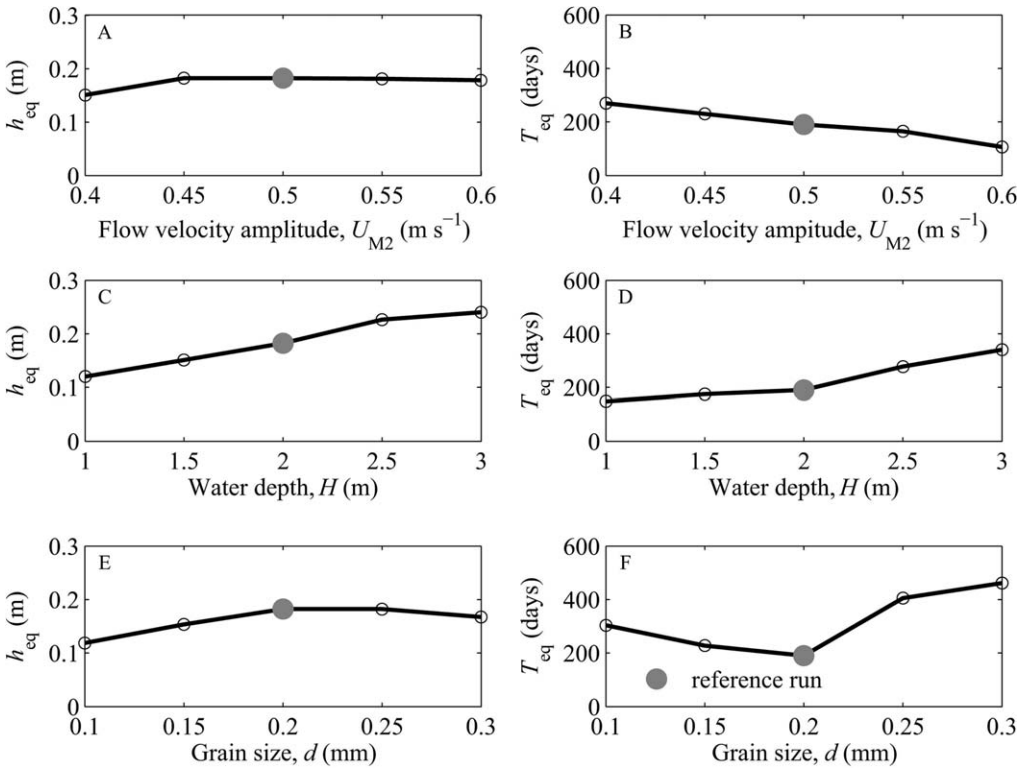

Fig. 8. Sensitivity in (A, C, E) equilibrium mound height (h_{eq}) and (B, D, F) equilibrium time (T_{eq}) for a variation in (A, B) flow velocity amplitude (U_{M2}), (C, D) water depth (H), and (E, F) grain size (d). Tube density D_{tube} = 500 ind. m^{-2} and a tube length L_{tube} = 2.0 cm.

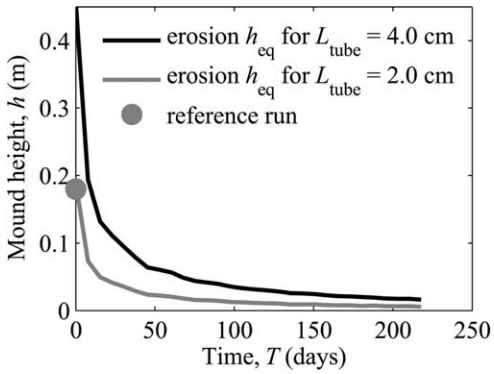

Fig. 9. Mound erosion for two different initial topographies. The initial topographies correspond to the equilibrium mound height for a population density of D_{tube} = 500 ind. m^{-2} and a tube length L_{tube} = 4.0 cm and L_{tube} = 2.0 cm.

characteristics in the intertidal environment are typically comparable with mound characteristics in the subtidal environment (Degraer et al. 2008; Rabaut et al. 2009). Therefore, we feel justified to compare intertidal field observations on mound height with subtidal model results, although future research should confirm this assumption. Not being able to include waves in our model might affect our estimates of the erosion time. Depending on the location, waves can form the major hydrodynamic force for destabilizing sediments in intertidal and shallow subtidal environments (Van der Molen 2002). Present results on erosion rates may hence not be applicable to wave-dominated environments. Moreover, the large extension of the mound outside the patch (Fig. 5) might be overestimated since waves are not included in the model. However, we think that the equilibrium mound height was not affected by the exclusion of waves. As found in a modeling study in the Dutch western Wadden Sea (Borsje et al. 2008), the bed shear stress by waves is sometimes as large as the bed shear stress produced by the tide. In our model simulations we varied the flow velocity amplitude and hence the bed shear stress by the tide from 0.38 N m^{-2} up to 0.85 N m^{-2} for a flow velocity variation of U_{M2} = 0.4 m s^{-1} to 0.6 m^{-1} respectively (Fig. 8A,B). For this doubling in bed shear stress, the equilibrium mound height hardly changed (Fig. 8A), but the equilibrium time decreased considerably (Fig. 8B). Therefore, the formation time of the mounds will be shorter by considering waves due to the increase in total transport, but we expect that the equilibrium mound height will not be influenced. Moreover, stabilizing organisms like diatoms found within the patch in the field are assumed to bind the sediment together and therefore increase the critical bed shear stress for erosion (Eckman et al. 1981). An increase in critical bed shear with 60% due to stabilizing organisms is found in areas near the mean water line, on the basis of field measurements in the Dutch western Wadden Sea executed by Cadée and Hegeman (1974). In our model simulations we varied the critical bed shear stress for erosion indirectly. For a variation in grain size from d = 0.1 mm to 0.3 mm we indirectly varied the critical bed shear stress for erosion from 0.13 N m^{-2} to 0.21 N m^{-2}. For such an increase, comparable with that of stabilizing organisms, the equilibrium mound height hardly showed any variation (Fig. 8E), but the formation time was much longer (Fig. 8F). Therefore, we expect that stabilizing organisms will not influence the equilibrium mound height, but will increase formation time of the mounds due to a decrease in transport rates.

As described in the introduction, results from flume studies are in many cases contradictory to field observations. Whereas flume studies show net sediment flux switched from erosion to a deposition above a coverage density of 5% (Friedrichs et al. 2000, 2009; Friedrichs and Graf 2009), field observations show mound presence for coverage densities even lower than 5% (Rabaut et al. 2009). On the basis of our results we can clarify these apparent contradictory trends. (1) In the field the flow direction reverses after half a tidal period. In the flume experiment by Friedrichs et al. (2000) erosion throughout the whole tube array was observed only until a coverage density of 2%. For high coverage densities, erosion was observed only near the leading edge of the patch. Inside and at the back of the patch, the bed level was unaffected. Since the location of the leading edge switches during reversing tidal periods, the erosion at the leading edge during ingoing tide is compensated by the accretion during outgoing tide. (2) The bed roughness outside the patch was much smaller in the flume experiments compared with field conditions. Therefore, flow velocities inside the patch were much larger in the flume studies and could therefore induce erosion, which was not observed in the field. (3) In the flume experiments the distribution of tube-building worms was regular and the tube length was constant. However, in the field the distribution of tube-building worms and the tube length are much more variable. Consequently, energy dissipation in the field is assumed to be much higher for randomly distributed tubes compared with the energy dissipation when tubes are regularly distributed. (4) In the flume experiments no bedload transport and suspended load transport outside the patch was accounted for. The model results showed an increase in bed shear stress outside the patch and hence erosion of sediment. This sediment settles within the patch because of a reduction in flow velocity.

The results of the model showed the ecosystem engineering capacity of the tube-building worm *L. conchilega*. For low population densities the flow velocities within the patch were strongly reduced and hence sediment accretion was enhanced. As recruitment within a patch is much larger than outside a patch (Strasser and Pieloth 2001; Van Hoey 2006), these relatively strong effects caused by low densities of tube worms may initiate a positive feedback loop (Bouma et al. 2007; Van Wesenbeeck et al. 2007), resulting in an increase in population density and consequently an increase in mound height. However, the model results also indicated that there is a limit to this positive feedback. For a population density of tube-building worms exceeding around D_{tube} = 3000 ind. m^{-2} the accretion of sediment stopped (coverage density of 5%). Hence our model suggests that reefs will evolve to an equilibrium that is determined by the tube length and population density. Feedback responses are, however, not

yet explicitly included in the model and need to be pursued in future studies.

In nature, the patchy habitat consisting of mounds of tube-building worm *L. conchilega* evolves quite dynamically, as it is very dependent on recruitment for reef renewal. *L. conchilega* reefs can persist only for a long time through renewal of the population (Godet et al. 2011). The prolonged existence of the mound as a sort of "legacy" of the reef is important for pelagic larvae to settle (Rabaut et al. 2009). Our model results showed that the mound legacy can persist quite long even after a period in which worms are absent from the mounds (i.e., > 100 d; Fig. 9). Thus, protection of areas with mounds that are temporarily not inhabited by living worms against disturbing agents such as, e.g., bottom trawling is of utmost importance, because the legacy of these ecosystem-engineered structures can be long enough to facilitate future establishment.

Acknowledgments

This work was part of the Ph.D. research of the lead author, B.W.B., which was supported by the Dutch Technology Foundation and the Technology Program of the Dutch Ministry of Economic Affairs. Deltares funded part of the research and made its Delft3D software available. We acknowledge Lowie Hazen, Bert Sinke, Achmad Adhitya, and Jelmer Schellingerhout for assisting in the flume experiments and analysis. Comments from two anonymous reviewers were much appreciated.

References

Baas, A. C. W., and J. M. Nield. 2007. Modelling vegetated dune landscapes. Geophys. Res. Lett. **34:** L06405, doi:10.1029/2006GL029152

Bobertz, B., J. Harff, and B. Bohling. 2009. Parameterisation of clastic sediments including benthic structures. J. Mar. Syst. **75:** 371–381, doi:10.1016/j.jmarsys.2007.06.010

Borsje, B. W., M. B. De Vries, T. J. Bouma, G. Besio, S.J.M.H. Hulscher, and P. M. J. Herman. 2009*a*. Modelling biogeomorphological influences for offshore sandwaves. Cont. Shelf Res. **29:** 1289–1301, doi:10.1016/j.csr.2009.02.008

———, ———, S. J. M. H. Hulscher, and G. J. De Boer. 2008. Modeling large scale cohesive sediment transport with the inclusion of biological activity. Est. Coastal Shelf Sci. **78:** 468–480, doi:10.1016/j.ecss.2008.01.009

———, S. J. M. H. Hulscher, P. M. J. Herman, and M. B. De Vries. 2009*b*. On the parameterization of biological influences on offshore sandwave dynamics. Ocean Dyn. **59:** 659–670, doi:10.1007/s10236-009-0199-0

———, W. M. Kranenburg, P. C. Roos, J. Matthieu, and S.J.M.H. Hulscher. 2014. The role of suspended load transport in the occurrence of tidal sand waves. J. Geophys. Res. **119:** 1–16, doi:10.1002/2013JF002828

———, P. C. Roos, W. M. Kranenburg, and S.J.M.H. Hulscher. 2013. Modelling sand wave formation in a numerical shallow water model: The role of turbulence formulation. Cont. Shelf Res. **60:** 17–27, doi:10.1016/j.csr.2013.04.023

Bouma, T. J., M. B. De Vries, and P. M. J. Herman. 2010. Comparing ecosystem engineering efficiency of 2 plant species with contrasting growth strategies. Ecology **91:** 2696–2704, doi:10.1890/09-0690

———, ———, E. Low, G. Peralta, I. C. Tanczos, J. Van de Koppel, and P. M. J. Herman. 2005. Trade-offs related to ecosystem-engineering: A case study on stiffness of emerging macrophytes. Ecology **86:** 2187–2199, doi:10.1890/04-1588

———, L. A. Van Duren, S. Temmerman, T. Claverie, A. Blanco-Garcia, T. Ysebaert, and P. M. J. Herman. 2007. Spatial flow and sedimentation patterns within patches of epibenthic structures: Combining field, flume and modeling experiments. Cont. Shelf Res. **27:** 1020–1045, doi:10.1016/j.csr.2005.12.019

Cadée, G. C., and J. Hegeman. 1974. Primary production of the benthic microflora living on tidal flats in the Dutch Wadden Sea. Neth. J. Sea Res. **8:** 260–291, doi:10.1016/0077-7579(74)90020-9

Carey, D. A. 1987. Sedimentological effects and palaeoecological implications of the tube-building polychaete *Lanice conchilega* Pallas. Sedimentology **34:** 49–66, doi:10.1111/j.1365-3091.1987.tb00559.x

Corenblit, D., and others. 2011. Feedbacks between geomorphology and biota controlling Earth surface processes and landforms: A review of foundation concepts and current understandings. Earth Sci. Rev. **106:** 307–311, doi:10.1016/j.earscirev.2011.03.002

D'Alpaos, A., S. Lanzoni, M. Marani, A. Bonornetto, G. Cecconi, and A. Rinaldo. 2007. Spontaneous tidal network formation within a constructed salt marsh: Observations and morphodynamic modelling. Geomorphology **91:** 186–197, doi:10.1016/j.geomorph.2007.04.013

Degraer, S., A. Volckaert, and M. Vincx. 2003. Macrobenthic zonation patterns along a morphodynamical continuum of macrotidal, low tide bar/rip and ultra-dissipative sandy beaches. Est. Coas. Shelf Sci. **56:** 459–468, doi:10.1016/S0272-7714(02)00195-6

———, and others. 2008. Very-high resolution side-scan sonar mapping of biogenic reefs of the tube-worm *Lanice conchilega*. Remote Sens. Environ. **112:** 3323–3328, doi:10.1016/j.rse.2007.12.012

Deltares 2014. User manual Delft-3D FLOW. Delft, the Netherlands.

Dijkstra, J. T., and R. E. Uittenbogaard. 2010. Modeling the interaction between flow and highly flexible aquatic vegetation. Water Resour. Res. **46:** W12547, doi:10.1029/2010WR009246

Eckman, J. E., A. R. M. Nowell, and P. A. Jumars. 1981. Sediment destabilization by animal tubes. J. Mar. Res. **39:** 361–374.

Friedrichs, M., and G. Graf. 2009. Characteristic flow patterns generated by macrozoobenthic structures. J. Mar. Syst. **75:** 348–359, doi:10.1016/j.jmarsys.2007.01.015

———, ———, and B. Springer. 2000. Skimming flow induced over a simulated polychaete tube lawn at low population densities. Mar. Ecol. Prog. Ser. **192:** 219–228, doi:10.3354/meps192219

———, T. Leipe, F. Peine, and G. Graf. 2009. Impact of macrozoobenthic structures on near-bed sediment fluxes. J. Mar. Syst. **75:** 336–347, doi:10.1016/j.jmarsys.2006.12.006

Godet, L., J. Fournier, M. Jaffre, and N. Desroy. 2011. Influence of stability and fragmentation of a worm-reef on benthic macrofauna. Est. Coast. Shelf Sci. **92:** 472–479, doi:10.1016/j.ecss.2011.02.003

Graf, G., and R. Rosenberg. 1997. Bioresuspension and biodeposition: A review. J. Mar. Syst. **11:** 269–278, doi:10.1016/S0924-7963(96)00126-1

Hastings, A., and others. 2007. Ecosystem engineering in space and time. Ecol. Lett. **10:** 153–164, doi:10.1111/j.1461-0248.2006.00997.x

Herman, P. M. J., J. J. Middelburg, and C. H. R. Heip. 2001. Benthic community structure and sediment processes on an intertidal flat: Results from the ECOFLAT project. Cont. Shelf Res. **21:** 2055–2071, doi:10.1016/S0278-4343(01)00042-5

Jones, C. G. 2012. Ecosystem engineers and geomorphological signatures in landscapes. Geomorphology **157–158:** 75–87, doi:10.1016/j.geomorph.2011.04.039

———, J. L. Gutierrez, J. E. Byers, J. A. Crooks, J. G. Lambrinos, and T. S. Talley. 2010. A framework for understanding physical ecosystem engineering by organisms. Oikos **119:** 1862–1869, doi:10.1111/j.1600-0706.2010.18782.x

———, J. H. Lawton, and M. Shachak. 1994. Organisms as ecosystem engineers. Oikos **69:** 373–386, doi:10.2307/3545850

———, ———, and ———. 1997. Positive and negative effects of organisms as physical ecosystem engineers. Ecology **78:** 1946–1957, doi:10.1890/0012-9658(1997)078[1946:PANEOO]2.0.CO;2

Kirwan, M. L., and A. B. Murray. 2007. A coupled geomorphic and ecological model of tidal marsh evolution. Proc. Natl. Acad. Sci. USA **104:** 6118–6122, doi:10.1073/pnas.0700958104

Le Hir, P., Y. Monbet, and F. Orvain. 2007. Sediment erodability in sediment transport modelling: Can we account for biota effects? Cont. Shelf Res. **27:** 1116–1142, doi:10.1016/j.csr.2005.11.016

Lesser, G. R., J. A. Roelvink, J. A. T. M. Van Kester, and G. S. Stelling. 2004. Development and validation of a three-dimensional morphological model. Coast. Eng. **51:** 883–915, doi:10.1016/j.coastaleng.2004.07.014

Murray, A. B., M. A. F. Knaapen, M. Tal, and M. L. Kirwan. 2008. Biomorphodynamics: Physical–biological feedbacks that shape landscapes. Water Resour. Res. **44:** W11301, doi:10.1029/2007WR006410

———, and C. Paola. 2003. Modeling the effect of vegetation on channel pattern in bedload rivers. Earth Surf. Proc. Landf. **28:** 131–143, doi:10.1002/esp.428

Nicolaidou, A. 2003. Observations on the re-establishment and tube construction by adults of the polychaete *Lanice conchilega*. J. Mar. Biol. Assoc. U.K. **83:** 1223–1224, doi:10.1017/S0025315403008531

Orvain, F., P. Le Hir, P. Sauriau, and S. Lefebvre. 2012. Modelling the effects of macrofauna on sediment transport and bed elevation: Application over a cross-shore mudflat profile and model validation. Est. Coast. Shelf Sci. **108:** 64–75, doi:10.1016/j.ecss.2011.12.036

Peralta, G., L. A. Van Duren, E. P. Morris, and T. J. Bouma. 2008. Consequences of shoot density and stiffness for ecosystem engineering by benthic macrophytes in flow dominated areas: A hydrodynamic flume study. Mar. Ecol. Prog. Ser. **368:** 103–115, doi:10.3354/meps07574

Rabaut, M. 2009. *Lanice conchilega*, fisheries and marine conservation: Towards an ecosystem approach to marine management. Ph.D. thesis. Ghent University.

———, K. Guilini, G. Van Hoey, M. Vincx, and S. Degraer. 2007. A bio-engineered soft-bottom environment: The impact of *Lanice conchilega* on the benthic species-specific densities and community structure. Est. Coastal Shelf Sci. **75:** 525–536, doi:10.1016/j.ecss.2007.05.041

———, M. Vincx, and S. Degraer. 2009. Do *Lanice conchilega* (sandmason) aggregations classify as reefs? Quantifying habitat modifying effects. Helg. Mar. Res. **63:** 37–46, doi:10.1007/s10152-008-0137-4

Reinhardt, L., D. Jerolmack, B. J. Cardinale, V. Vanacker, and J. Wright. 2010. Dynamic interactions of life and its landscape: Feedbacks at the interface of geomorphology and ecology. Earth Surf. Proc. Landf. **35:** 78–101, doi:10.1002/esp.1912

Strasser, M., and U. Pieloth. 2001. Recolonization pattern of the polychaete *Lanice conchilega* on an intertidal sand flat following the severe winter of 1995/96. Helg. Mar. Res. **55:** 176–191, doi:10.1007/s101520100081

Tal, M., and C. Paola. 2007. Dynamic single-thread channels maintained by the interaction of flow and vegetation. Geology **35:** 347–350, doi:10.1130/G23260A.1

Temmerman, S., T. J. Bouma, G. Govers, Z. B. Wang, M. B. De Vries, and P. M. J. Herman. 2005. Impact of vegetation on flow routing and sedimentation patterns: Three-dimensional modeling for a tidal marsh. J. Geophys. Res. **110:** F04019, doi:10.1029/2005JF000301

———, ———, J. Van de Koppel, D. Van der Wal, M. B. De Vries, and P. M. J. Herman. 2007. Vegetation causes channel erosion in a tidal landscape. Geology **35:** 631–634, doi:10.1130/G23502A.1

Van der Molen, J. 2002. The influence of tides, wind and waves on the net sand transport in the North Sea. Cont. Shelf Res. **22:** 2739–2762, doi:10.1016/S0278-4343(02)00124-3

Van Hoey, G. 2006. Spatio-temporal variability within the macrobenthic *Abra alba* community, with the emphasis on the structuring role of *Lanice conchilega*. Ph.D. thesis. Ghent University.

Van Hulzen, J. B., J. Van Soelen, and T. J. Bouma. 2007. Morphological variation and habitat modification are strongly correlated for the autogenic ecosystem engineer *Spartina anglica* (common cordgrass). Est. Coast **30:** 3–11, doi:10.1007/BF02782962

Van Rijn, L. C., D. J. R. Walstra, and M. Van Ormondt. 2004. Description of TRANSPOR 2004 (TR2004) and implementation in DELFT3D online. Report Z3748, Delft Hydraulics, Delft, The Netherlands.

———. 2007. Unified view of sediment transport by currents and waves. II: Suspended transport. J. Hydraul. Eng. **133:** 668–689, doi:10.1061/(ASCE)0733-9429(2007)133:6(668)

Van Wesenbeeck, B. K., J. Van de Koppel, P. M. J. Herman, and T. J. Bouma. 2007. Does scale-dependent feedback explain spatial complexity in salt-marsh ecosystems? Oikos **117:** 152–159, doi:10.1111/j.2007.0030-1299.16245.x

Verfaillie, E., V. Van Lancker, and M. Van Meirvenne. 2006. Multivariate geostatistics for the predictive modeling of the surficial sand distribution in shelf seas. Cont. Shelf Res. **26:** 2454–2468, doi:10.1016/j.csr.2006.07.028

Widdows, J., and M. D. Brinsley. 2002. Impact of biotic and abiotic processes on sediment dynamics and the consequences to the structure and functioning of the intertidal zone. J. Sea Res. **48:** 143–156, doi:10.1016/S1385-1101(02)00148-X

Associate editor: Bo Thamdrup

Received: 31 October 2013
Accepted: 28 January 2014
Amended: 17 February 2014